Crack propagation in non-homogenous materials: Evaluation of mixed-mode SIFs, T-stress and kinking angle using a variant EFG method

Muthu, N., Maiti, S. K., Falzon, B. G., & Yan, W. (2016). Crack propagation in non-homogenous materials: Evaluation of mixed-mode SIFs, T-stress and kinking angle using a variant EFG method. Engineering Analysis with Boundary Elements, 72, 11-26. DOI: 10.1016/j.enganabound.2016.07.017

Published in:
Engineering Analysis with Boundary Elements

Document Version:
Early version, also known as pre-print

Crack Propagation in Non-homogenous materials: Evaluation of Mixed-Mode SIFs, T-stress and Kinking angle using a variant of EFG Method

N. Muthu[a,b,d], S.K. Maiti[b], B.G. Falzon[c], Wenyi Yan[d]

[a] *IITB-Monash Research Academy, CSE Building, 2nd Floor, IIT Bombay, Powai, 400076, India.*
[b] *Department of Mechanical Engineering, IIT Bombay, Powai, 400076, India. Email id: skmaiti@iitb.ac.in, phone:* +91-22-2576-7526, *fax:* +91-22-2572-6875.
[c] *School of Mechanical and Aerospace Engineering, Queen's University Belfast, Belfast, BT9 5AH, UK.*
[d] *Department of Mechanical and Aerospace Engineering, Monash University, Clayton, VIC 3800, Australia.*

ABSTRACT

A new variant of the Element-Free Galerkin (EFG) method, that combines the diffraction method, to characterize the crack tip solution, and the Heaviside enrichment function for representing discontinuity due to a crack, has been used to model crack propagation through non-homogenous materials. In the case of interface crack propagation, the kink angle is predicted by applying the maximum tangential principal stress (MTPS) criterion in conjunction with consideration of the energy release rate (ERR). The MTPS criterion is applied to the crack tip stress field described by both the stress intensity factor (SIF) and the T-stress, which are extracted using the interaction integral method. The proposed EFG method has been developed and applied for 2D case studies involving a crack in an orthotropic material, crack along an interface and a crack terminating at a bi-material interface, under mechanical or thermal loading; this is done to demonstrate the advantages and efficiency of the proposed methodology. The computed SIFs, T-stress and the predicted interface crack kink angles are compared with existing results in the literature and are found to be in good agreement. An example of crack growth through a particle-reinforced composite materials, which may involve crack meandering around the particle, is reported.

KEY WORDS: *EFG, SIF, T-stress, interface crack, MTPS, crack propagation*.

1. INTRODUCTION

Composite materials are often subjected to extreme mechanical and thermal loading conditions that make them susceptible to damage through crack formation. Studies on the modelling of fracture in composites, range from nanoscale to macroscale analysis. Useful insight into the study of fracture may be gained through analysis at the microscale. At this level, the constituent materials are represented separately, i.e. the material is non-homogenous usually consisting of dissimilar materials or bi-materials separated by an interface [1].

A propagating crack at the microscale may often impinge on the bi-material interface at an angle. The associated singular stress field consists of two different orders of singularity which may be either complex conjugates or real [2-3]. In addition, a crack tip that meets an interface of two materials may grow along it or penetrate into the neighbouring material. The criterion for such a crack to kink into the neighbouring material is different from the criterion governing the crack propagation in a homogenous material. The development of a proper numerical

method and an efficient approach to predict the angle of crack propagation, including kinking of an interface crack, can be very useful in the study of fracture of composites.

Mesh-based methods like the finite element method (FEM) and the boundary element method (BEM) pose difficulties for crack propagation problems due to extensive meshing and re-meshing. Although the extended finite element method (XFEM), based on the partition-of-unity approach, eliminated some of the difficulties, the enrichment functions depend on the crack tip location in non-homogenous materials [4-8]. Meshfree methods (MMs) [9-10] provide alternatives to study such problems. The EFG method [11], whose shape functions are higher order continuous, has been shown to be very useful for fracture mechanics applications [12-17]. A variety of enrichment strategies [18-22], within the realm of EFG method, have been proposed to model crack in homogenous material. The choice of EFG method that can offer advantages in modelling crack propagation through non-homogenous materials is limited. Development of new schemes can be helpful. This has provided some motivation for the present study.

Williams and Ewing [23], Finnie and Saith [24], Ewing and Williams [25], Ueda et al. [26], and Cotterell [27] proposed the use of T-stress of the power series expansion of the stress distribution due to a crack, to determine the crack paths in metals under pure mode I loading. Since then, many investigators [28-31], used the T-stress on top of the singular stress field to predict crack paths. Matvienko [32] reported good agreement between predicted fracture angles and experimental data for mixed-mode I/II crack growth through Guiting limestone. Ki [33] studied the existing criteria for crack kinking out of an interface and recommended the use of the T-stress. To the authors' knowledge, no studies have been reported concerning the use of T-stress on the crack propagation through non-homogenous materials, within the framework of MMs.

There are several criteria to determine the instantaneous angle of crack propagation when the crack is in a homogenous medium. However only few criteria have been proposed to predict this kinking angle [33] in the case of an interface crack. He and Hutchinson [34] indicated that an interface crack would penetrate the adjoining material depending on the energy release rate (ERR) associated with the kinking direction and the relative toughness of the interface and the neighbouring material. The competition between penetration and deflection of a crack also depended on the ratio of kinked crack extension lengths. To overcome this difficulty, a revised energy based criterion was developed and applied to composite problems [35-41]. Akisanya and Fleck [42] explained the zigzag propagation of a crack within a layer sandwiched between two tougher materials in terms of the mode II stress intensity factor $K_{II} = 0$. The determination of the interface crack kinking angle, using the ERR criterion and $K_{II} = 0$ criterion, requires multiple case studies, which is computationally costly. Amestoy and Leblond [43] have compared the differences between the energy release rate criterion and $K_{II} = 0$ criterion.

Yuuki and Xu [44] proposed a criterion based on the maximum tangential stress (MTS) given only by the singularity term and compared the results with experimental data. In the MTS criterion given in reference, the first term of the eigenfunction expansion, or the singularity term, is only used to determine the angle of crack propagation. This angle corresponds to the direction of maximum tangential principal stress. The crack propagation angle given by the MTS criterion does not correspond to a principal direction when higher order terms are also used. In such a case, the direction given by $\tau_{r\theta} = 0$ corresponds to a principal direction. This criterion, termed as zero shear stress criterion, or MTPS criterion [45], was implemented in the case of homogenous materials. Application of such a criterion is convenient and it helps to avoid analyses of multiple cases to determine the interface crack kinking angle. Its application

to bi-material interface cracks has not yet been reported.

The present paper examines the possibility of developing a variant of the EFG method plus the applicability of the MTPS criterion, in conjunction with the ERR technique, for modelling crack propagation through non-homogenous materials.

The outline of the paper is as follows: The proposed EFG method formulation with crack modelling techniques is detailed in Section 2. In Section 3, the interaction integral used to extract mixed mode SIFs and T-stress is described. The modified interaction integral, to handle the situation when the crack tip is close to a bi-material interface, is also presented. Section 4 discusses the proposed criterion combining the concepts of a stress based criterion and the ERR to predict the kinking angle of an interface crack. The convergence study is presented in Section 5. In Section 6, these schemes have been applied to a number of problems, including thermal load problems, to illustrate their performance. The influence of the T-stress on the kinking angle has been also examined. This is followed by some concluding remarks in Section 7.

2. MODIFIED EFG METHOD

In the displacement-based EFG method, the displacement at location $\mathbf{x}$ within a support domain of n nodes, $\mathbf{u}(\mathbf{x})$, can be represented as

$$\mathbf{u}(\mathbf{x}) = \sum_{I=1}^{n} \Phi_I(\mathbf{x})\mathbf{u}_I \tag{1}$$

where $\Phi_I(\mathbf{x})$ are the nodal shape functions and $\mathbf{u}_I$ are the nodal displacement vectors. The moving least squares (MLS) interpolation [46] technique is used to develop the shape functions in the EFG method.

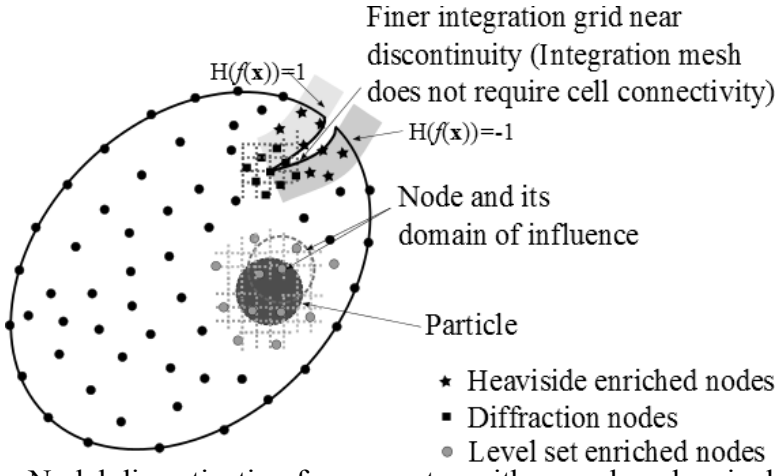

Fig. 1. Nodal discretization for geometry with a crack and an inclusion.

In this work, the Heaviside function is used to take care of the discontinuity between the crack edges and the diffraction method is used in the region around the crack tip. The diffraction method eliminates the need of enrichment functions that depend on the location of the crack tip, orientation of the crack to a material interface and material properties. The Heaviside function helps to avoid the need of adding additional nodes along the crack faces in a problem of mixed-mode crack propagation. Consequently, the displacement approximation in the proposed EFG method in the presence of a crack (strong discontinuity) and inclusion boundary (weak discontinuity) present in a given geometry (Fig. 1), takes the form

$$\mathbf{u}(\mathbf{x}) = \sum_{I\in w(\mathbf{x})} \Phi_I(\mathbf{x})\mathbf{u}_I + \sum_{I\in w_j(\mathbf{x})} \Phi_I(\mathbf{x})\{\mathbf{a}_I \mathrm{H}(f(\mathbf{x}))\} + \sum_{I\in w_c(\mathbf{x})} \Phi_I(\mathbf{x})\mathbf{c}_I\chi_I(\mathbf{x}) \tag{2}$$

where function $\chi_I(\mathbf{x}) = \mathrm{F}^1(\mathbf{x}) - \mathrm{F}^1(\mathbf{x}_I)$ is employed for displacement continuity across the

interface with $\mathrm{F}^{\mathrm{I}}(\mathbf{x}) = \sum_{I \in w_c(\mathrm{x})} |\zeta_I| \Phi_I(\mathbf{x}) - \left| \sum_{I \in w_c(\mathrm{x})} \zeta_I \Phi_I(\mathbf{x}) \right|$. ζ_I is the signed distance of node *I* from the interface [47]. The set $w(\mathbf{x})$ consists of nodes in the support domain of $\mathbf{x}$. The set $w_j(\mathbf{x})$ and $w_c(\mathbf{x})$ consist of Heaviside enriched and level set enriched nodes with a displacement continuity function. This method may not capture the order of the singularity exactly. However, the higher order nodal shape functions ensure an accurate and easier computation of the SIFs.

The routinely used polynomial basis $\mathrm{p} = [1 \; x \; y]$ needed for the development of shape functions of the EFG method through the MLS technique, is employed. The cubic B-spline weight function with circular domain of influence is used. For accurate integration purposes, the background mesh that intersects the crack is subdivided into triangles such that no mesh crisscrosses the crack [48], as shown in Fig. 2. In the present work, in addition to the sub-triangulation, a 13th order Gauss quadrature has been used in each triangle close to the crack tip for integration.

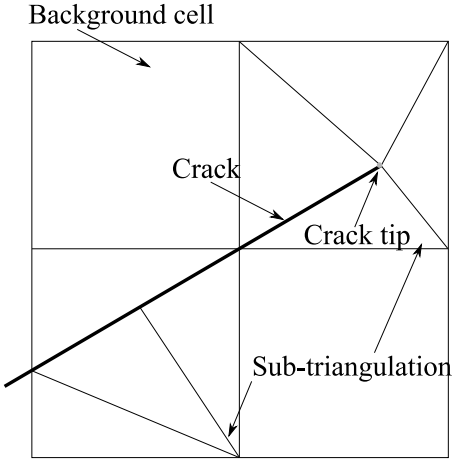

Fig. 2. Sub-triangulation for the background mesh.

3. INTERACTION INTEGRAL TO EXTRACT SIFs AND T-STRESS

There exist variety of post processing techniques, within the framework of the EFG method, to compute the SIFs for a crack in isotropic and homogenous materials [48,49] and complex SIF for an interface crack [50-55]. The popular interaction integral/M-integral [56] technique is used to extract the complex SIF associated with an interface crack under mechanical and thermal loading. The same interaction integral is also used to extract the T-stress with the help of different auxiliary functions [57]. A modified interaction integral [58] is used to extract mixed-mode SIFs for a crack when it is close to material interfaces.

For a crack in a homogenous material under thermal (ΔT) field and crack face loading, the interaction integral is given by

$$I = \int_A (\sigma_{ij} u_{i,1}^{aux} + \sigma_{ij}^{aux} u_{i,1} - \sigma_{ik} \varepsilon_{ik}^{aux} \delta_{1j}) q_{,j} dA - \int_{\Gamma_{c+}+\Gamma_{c-}} t_{cj} u_{j,1}^{aux} q d\Gamma + \varphi \int_A \varepsilon_{kk}^{aux} (\Delta T)_{,1} q dA$$

$$\varphi = \begin{cases} E\eta/(1-2\nu) & \text{for plane strain} \\ E\eta/(1-\nu) & \text{for plane stress} \end{cases} \tag{3}$$

where A is the area of integration as shown in Fig. 3(a). E, η and ν are, respectively, Young's modulus, thermal coefficient of expansion and Poisson's ratio. q is a scalar function which has the value of unity on the contour S_1 and zero on S_2. δ_{ij} is the Kronecker's delta. The integration is carried out by shrinking the area A_o to zero. In evaluating the energy release rate in the

absence of crack face tractions, the second term in Eq. (3) is omitted. $\sigma_{ij}^{aux}, \varepsilon_{ik}^{aux}$ and u_i^{aux} are auxiliary state solutions; they correspond to the theoretical crack tip solution in a homogenous material.

For a crack in an isotropic and homogenous material, the interaction integral/M-integral can be expressed in terms of mixed-mode SIFs as follows:

$$I = \frac{(2K_I K_I^{aux} + 2K_{II} K_{II}^{aux})}{E^*} \tag{4}$$

where E^* is E for plane stress and $E/(1\text{-}\nu^2)$ for plane strain. K_I is evaluated by setting K_I^{aux} to unity and K_{II}^{aux} to zero. Similarly K_{II} is evaluated by setting K_{II}^{aux} to unity and K_I^{aux} to zero.

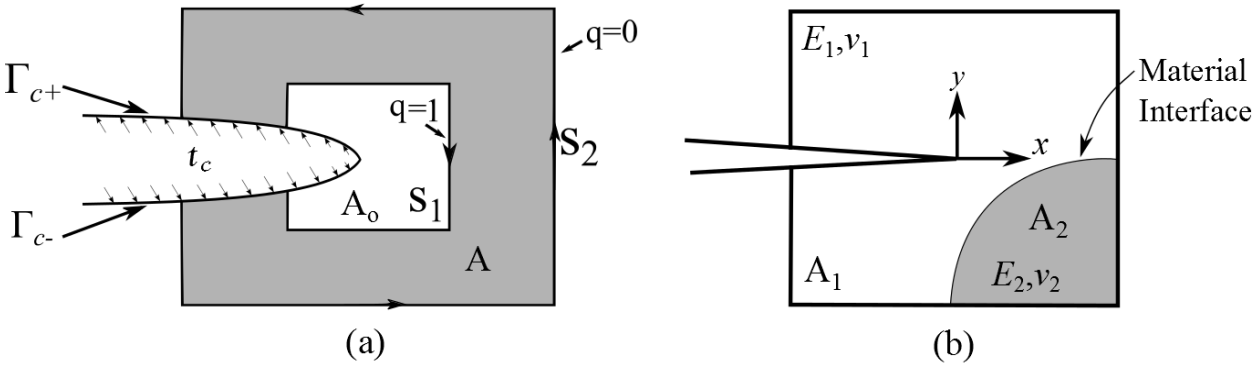

Fig. 3. (a) Area for domain integral; **(b)** Domain of integration consisting of material interfaces.

The interaction integral, devoid of a crack face and thermal loading, consists of an extra term when the domain of integration consists of a bi-material interface, as shown in Fig. 3(b). This is given [58] by

$$I = \int_A (\sigma_{ij} u_{i,1}^{aux} + \sigma_{ij}^{aux} u_{i,1} - \sigma_{ik} \varepsilon_{ik}^{aux} \delta_{1j}) q_{,j} dA + \int_A \sigma_{ij} \{S_{ijkl}^{tip} - S_{ijkl}(\mathbf{x})\} \sigma_{kl,1}^{aux} q dA \tag{5}$$

where $A = A_1 \cup A_2$. S_{ijkl}^{tip} is the compliance tensor at the crack tip and $S_{ijkl}(\mathbf{x})$ is the compliance tensor at a generic point $\mathbf{x}$. The generic point can lie in domain A_1 or A_2.

3.1 Mixed-Mode SIFs for Bi-materials

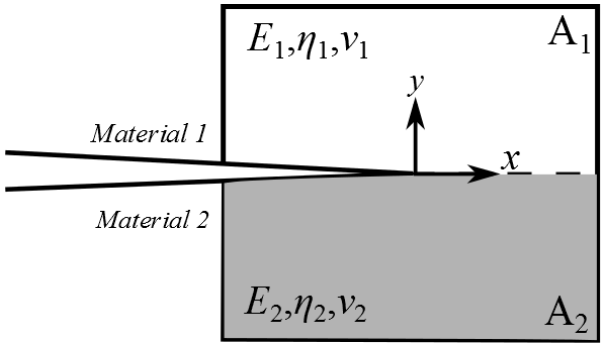

Fig. 4. Interaction integral domain for interface crack.

In the case of an interface crack in bi-materials (Fig. 4) subjected to mechanical and thermal load, ΔT, the interaction integral [59] is given by

$$I = \sum_{m=1}^{2} \int_{A_m} (\sigma_{ij} u_{i,1}^{aux} + \sigma_{ij}^{aux} u_{i,1} - \sigma_{ik} \varepsilon_{ik}^{aux} \delta_{1j}) q_{,j} dA + \sum_{m=1}^{2} \varphi_m \int_{A_m} \varepsilon_{kk}^{aux} (\Delta T)_{,1} q dA \tag{6}$$

$\sigma_{ij}^{aux}, \varepsilon_{ik}^{aux}$ and u_i^{aux} are obtained from the crack tip solutions for an auxiliary state with an interface crack. The complex SIF can be computed through the following relation,

$$I = \frac{(1/E_1^* + 1/E_2^*)(2K_1K_2^{aux} + 2K_2K_2^{aux})}{2\cosh^2(\pi\varepsilon)} \tag{7}$$

ε is the bi-material oscillatory parameter given by,

$$\varepsilon = \frac{1}{2\pi}\ln\left(\frac{1-\beta}{1+\beta}\right) = \frac{1}{2\pi}\ln\left(\frac{\kappa_1\mu_2 + \mu_1}{\kappa_2\mu_1 + \mu_2}\right)$$
$$\beta = \frac{1}{2}\left[\frac{\mu_1(1-2\nu_2) - \mu_2(1-2\nu_1)}{\mu_1(1-\nu_2) + \mu_2(1-\nu_1)}\right] \tag{8}$$

where μ_m is the shear modulus and κ_m is the Kolosov's constant, m = 1 and 2. κ_m is $(3-4\nu_m)$ in the case of plane strain and $(3-\nu_m)/(1+\nu_m)$ in the case of plane stress. β is second Dundurs' parameter. The stress intensity factor amplitudes, K_1 and K_2, associated with an interface crack are different from mode I and mode II SIFs for a crack in isotropic and homogenous material. The dimension of $\mathbf{K} = K_1 + iK_2$ is $\text{MPa(m)}^{0.5-i\varepsilon}$; the dimension of mode I (K_I) or mode II SIF (K_{II}) is $\text{MPa(m)}^{0.5}$.

3.2 T-stress for bi-material interface crack

The stress state for an interface crack is given by

$$\sigma_{ij}^m = \frac{F_{ij}^m(\theta)}{\sqrt{r}}\text{Re}\left[\mathbf{K}r^{i\varepsilon}\right] + \frac{G_{ij}^m(\theta)}{\sqrt{r}}\text{Im}\left[\mathbf{K}r^{i\varepsilon}\right] + T_m\delta_{i1}\delta_{j1} + O(\sqrt{r}) \tag{9}$$

where $\mathbf{K} = K_1 + iK_2$ (complex SIF) and T_m is the T-stress for material m, m = 1 and 2. T-stress represents the first non-singular stress term of the William's eigenfunction expansion of a crack tip stress field. The angular functions $F_{ij}^m(\theta)$ and $G_{ij}^m(\theta)$ are given in refs. [60] and [58].

The same Eq. (6) is invoked to determine the T-stress. It is possible only through the selection of appropriate auxiliary stresses (σ_{ij}^{aux}), strains (ε_{ik}^{aux}) and displacements (u_i^{aux}) in the integral. The auxiliary functions are given in Appendix A. The T-stress is related to the interaction integral by

$$T_m = \frac{IE_m^*}{f} \tag{10}$$

where T_m is the T-stress in the material m and f is a point force applied. The auxiliary field corresponds to this force. The same auxiliary solution with $m = 1$ can be used to determine the T-stress through Eq. (5) for a crack inside an isotropic material.

4. CRITERIA FOR PREDICTION OF DIRECTION OF CRACK PROPAGATION

He and Hutchinson [34] proposed that the kink angle ω of an interface crack (Fig. 5(a)) is dictated by the maximum energy release rate (ERR) of the kinked crack. In order to find the

maximum energy release rate $G_{m\omega}$, the crack is extended by Δa in various direction, θ, as shown in Fig. 5(b). Δa_d and Δa_p are deflected and penetrated kinked crack lengths respectively. The direction θ corresponding to the maximum energy release rate $G_{m\omega}$ is the angle of crack propagation, $\omega = \theta$, into the material m (#1 or #2).

The tendency of the interface crack to kink out of the interface or to grow along it is determined by

$$\frac{G_{m\omega}}{\Gamma_f^m} > \frac{G_I}{\Gamma_f^I} \tag{11}$$

where Γ_f^m and Γ_f^I are the fracture toughness of material *m* and the interface, respectively. The crack is likely to penetrate the homogenous neighbouring material if the inequality in Eq. (11) holds. Otherwise, it is likely to extend along the interface.

The ERR G_I along the interface and ERR $G_{m\omega}$ along the kinking angle ω are given by

$$\begin{aligned} G_I &= \frac{1}{E^*}\frac{K_1^2+K_2^2}{\cosh^2(\pi\varepsilon)} \\ G_{m\omega} &= \frac{1}{E_m^*}\frac{K_I^2+K_{II}^2}{2} \\ 1/E^* &= 1/E_1^* + 1/E_2^* \end{aligned} \tag{12}$$

where E_m^* is E_m for plane stress and $E_m/(1\text{-}\nu^2)$ for plane strain for the material m.

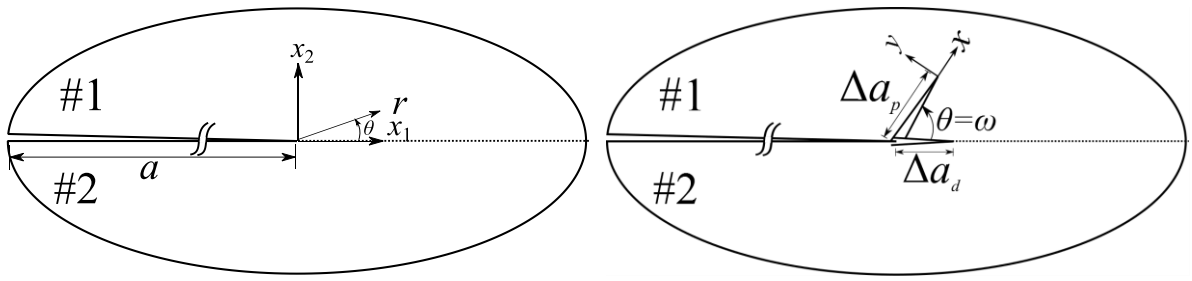

(a) (b)

Fig. 5. (a) Interface crack; **(b)** Kinking of an interface crack.

Although the energy-based criterion can be used to determine both the kinking angle and the load leading to initiation of kinking of an interface crack, it requires substantial computational effort. This is because the criterion requires multiple analyses to generate a variation of the ERR with possible kinking direction θ. In general, for an accurate computation of ERR, length Δa of the kinked crack is kept very small compared to the parent interface crack.

Yuuki and Xu [44] proposed that the interface crack would extend in the direction of maximum tangential/hoop stress given by the singularity term; they did not consider T-stress in their analysis. For evaluation of tangential stress ($\sigma_{\theta\theta}$), a circle of finite radius is considered (Fig. 6). The θ corresponding to $\sigma_{\theta\theta}^{\max}$ gives the kinking angle $\omega = \theta$. However, this criterion alone cannot determine whether the crack will kink into the material m or grow along the interface; this requires knowledge of the fracture toughness or fracture strength of the constitutive materials including the interface and the ERRs along possible kinking angle ω and the interface.

The zero K_{II} criterion, proposed by Akisanya and Fleck [42], stipulates that the interface crack kinks in the direction corresponding to $K_{II}=0$. The mixed-mode SIF of a kinked crack of length Δa is related to the parent crack by [34,42].

$$K_I + iK_{II} = c\mathbf{K}(\Delta a)^{i\varepsilon} + \bar{d}\mathbf{K}(\Delta a)^{i\varepsilon} + gT_m\sqrt{\Delta a} \tag{13}$$

$c, \bar{d}$ and g are complex functions that are dependent on material parameters α, β and kink angle ω. α is first Dundurs' parameter given by

$$\alpha = \frac{\mu_1(1-\nu_2)-\mu_2(1-\nu_1)}{\mu_1(1-\nu_2)+\mu_2(1-\nu_1)} \tag{14}$$

Given the complex functions $c, \bar{d}$ and g, the complex SIF of the interface crack, calculated from the interaction integral or any other SIF extraction technique is substituted in Eq. (13) to determine ω. In the absence of $c, \bar{d}$ and g data, the kinked crack of length Δa is extended in various directions, θ. The kink angle ω corresponds to the direction at which mode II SIF of the kinked crack is zero. This gives $\tau_{r\theta}=0$ for the kinked crack, not the original crack. This is in a sense *a posteriori* stress field criterion. Similar to the $\sigma_{\theta\theta}^{\max}$ criterion, this criterion too cannot determine whether the crack will penetrate or deflect without the knowledge of the individual fracture toughness of the constituent materials and of the interface plus the ERRs along these directions.

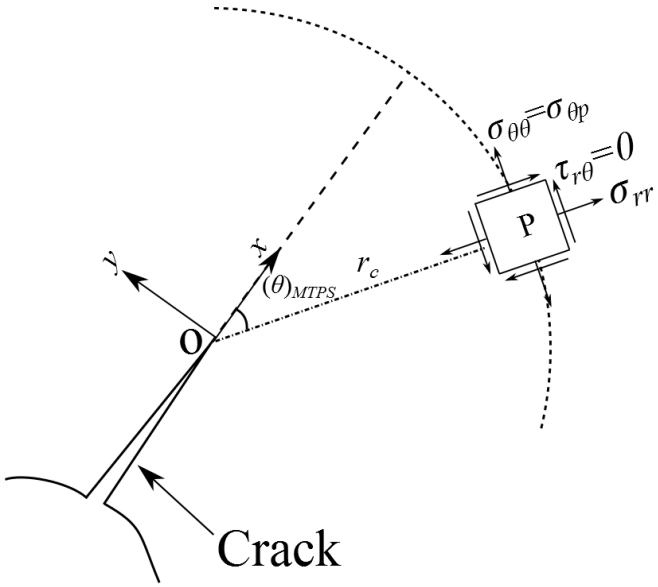

Fig. 6. Kinking angle of crack in homogenous medium.

In order to merge the advantages and overcome some of the difficulties, a criterion based on both the stress state and energy release rate is used here to predict the direction of kinking and the onset of crack propagation. The maximum tangential principal stress (MTPS) criterion is used as a stress criterion; according to the MTPS criterion, a crack extends in a radial direction corresponding to $\tau_{r\theta}=0$ [32,61]. The crack propagates when the maximum tangential stress at the location reaches a critical value, a property of the material. This is based on Rankine's maximum principal stress theory. This is similar to the $K_{II}=0$ criterion, but with a difference. In the MTPS criterion, the determination of kink angle ω is based on the *a priori* stress field due to the parent interface crack. However, in $K_{II}=0$ criterion, the kink angle ω is based on the main crack plus a kinked crack of length Δa.

The MTS criterion gives the direction of crack extension θ_{MTS} corresponding to $\partial\sigma_{\theta\theta}/\partial\theta = 0$, while the MTPS criterion gives the direction θ_{MTPS} corresponding to $\tau_{r\theta} = 0$. There will be a small difference between θ_{MTS} and θ_{MTPS}. $\sigma_{\theta\theta}$ for θ_{MTS} is the maximum tangential stress but not a principal stress $\sigma_{\theta p}$, but $\sigma_{\theta\theta}$ for θ_{MTPS} is not the maximum tangential stress but is the maximum tangential principal stress.

Although the condition in terms of stress may ensure breaking of material ligament ahead of the crack tip, the availability of energy must be sufficient for creation of the new surfaces. This implies that the stress criterion may indicate the direction of possible extension, the actual occurrence is decided by the energy release rate and the fracture toughness of the material.

Eq. (11) is dependent on the ratio of kinked lengths - Δa_d and Δa_p. When $\Delta a_d, \Delta a_p \to 0$, the ERRs are unrealistic i.e. G_I and $G_{m\omega}$ are zero or infinite depending upon the value of λ [35]. The crack extension length scales could be atomic, or larger depending upon the structural defects in the neighbourhood of the crack tip, whose determination is very difficult. Since the scope of the present work is limited to the application of the EFG method, an assumption is made such that $\Delta a = \Delta a_d = \Delta a_p$.

The advantages of combining the two criteria are: (1) It reduces the need of multiple analysis. The potential kink angle ω is obtained by the MTPS criterion. The ERR along the kink direction $G_{m\omega}$ can be obtained by extending a small crack Δa in the kink direction ω. Then, the ERR G_I associated with the in-plane extension for a parent interface crack and $G_{m\omega}$ are substituted in Eq. (11) to predict the crack extension direction. (2) The effect of T-stress is included in the stress-based criterion.

5. COVERGENCE STUDY

A plate of width, $w = 1\,\text{m}$, and a length to width ratio, $L/w = 2$, with an edge crack (a/w=0.5) is shown in Fig. 7(a). It is subjected to a traction of 1 MPa. The domain of influence is set at 1.75 times the regular nodal spacing. The materials is isotropic with a Young's modulus, $E = 210\,\text{GPa}$, and Poisson's ratio $\nu = 0.3$. The theoretical SIF for this case is $3.543\,\text{MPa}\sqrt{\text{m}}$ [62].

The % error in SIF obtained using the M-integral is plotted for various nodal discretizations, using different EFG methods based on: (1) eXtended element-free Galerkin (XEFG) method, (2) visibility, (3) diffraction and (4) present EFG method (Fig.7(b)). Notably, the XEFG method incorporates enrichment functions to model the crack-tip stress field [48]. The visibility and diffraction method involves modified weight functions around the crack tip. Their details are given in [49]. This plot shows that the present method decreases the % error in SIF with increasing nodal density. It has better accuracy compared to the visibility and diffraction methods. The improvement in the accuracy may be attributed to the coupling of the diffraction method with the Heaviside enrichment function.

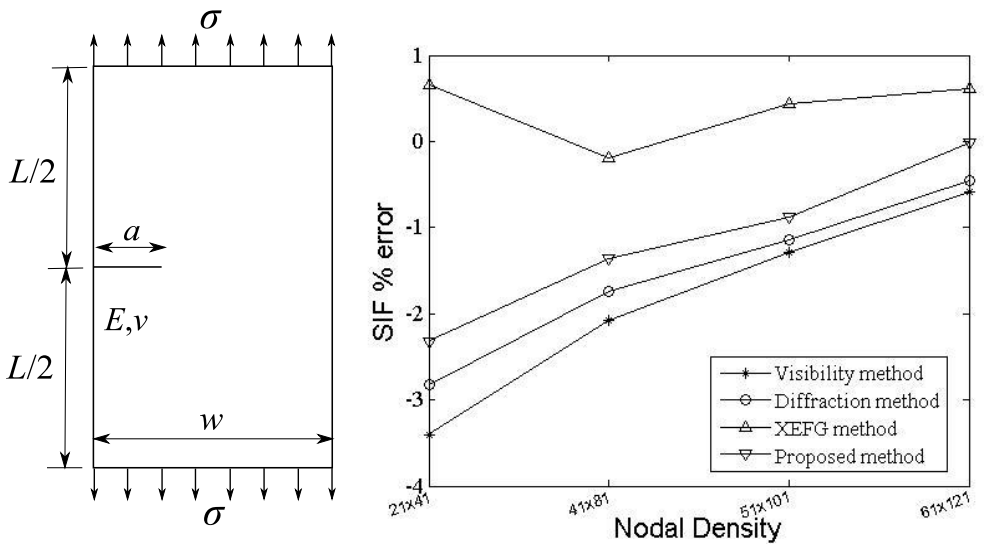

(a) (b)

Fig. 7. (a) A finite plate with an edge crack subjected to uniform tensile load; **(b)** SIF % error with nodal density.

The XEFG method performs better compared to the proposed method owing to the crack tip enrichment functions for lower nodal densities. However, when a nodal refinement is used in the region around the crack tip as shown in Fig. 8(a), there is a significant improvement.

Fig. 8(b) shows the convergence of SIF using a coarser nodal discretization of 21×41, and the present EFG method with various refinements in the region around the crack tip. It is observed that even with the usage of very low refinement 7×7, the SIF % error becomes less than 2%. As the refinement increases, the error decreases and the result converges to the exact solution. This is advantageous especially for modelling the crack propagation through non-homogenous materials because this eliminates the need of enrichment functions.

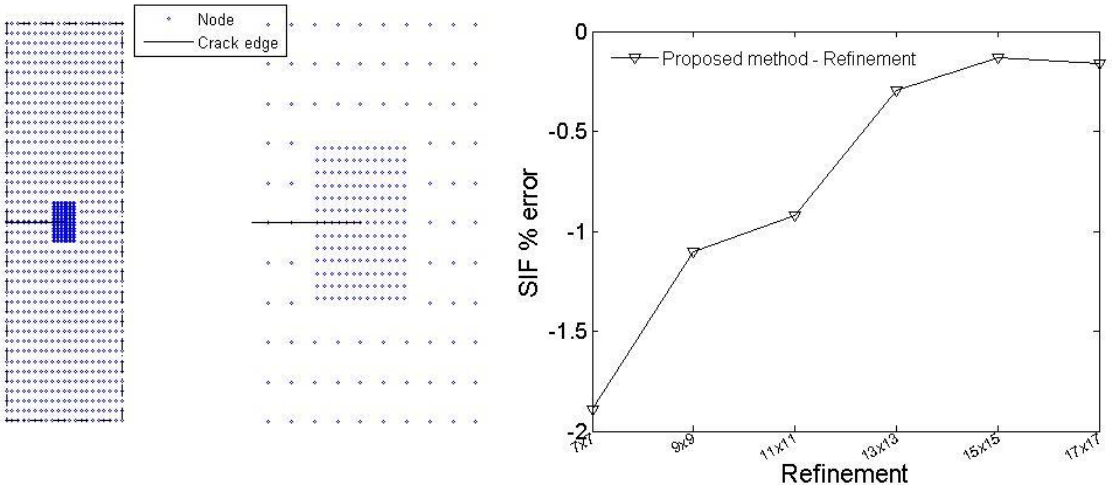

(a) (b)

Fig. 8. (a) Local refinement at the crack tip; **(b)** % error in SIF with refinement in the region around the crack tip, using the proposed method.

6. RESULTS AND DISCUSSIONS

6.1 Crack in an orthotropic material

Fig. 9(a) shows a square plate of a/w=0.1 with a centre crack aligned along its axis of orthotropy. The plate is subjected to a uniform tensile load of 1Pa. The material properties correspond to graphite-epoxy. A state of plane stress is assumed.

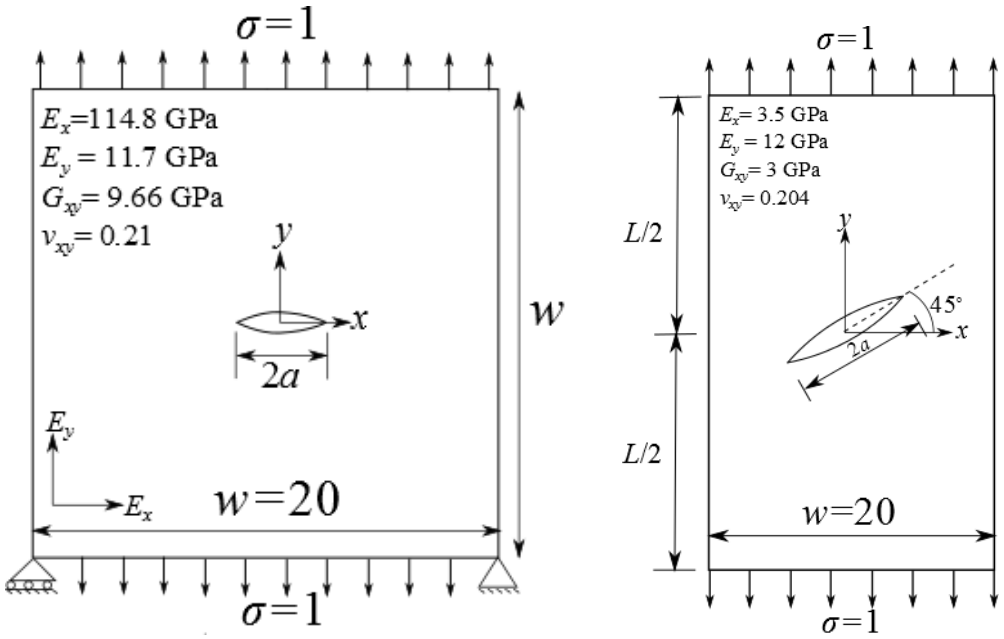

Fig. 9. (a) Crack in an orthotropic square plate; **(b)** Crack in an orthotropic rectangular plate.

A 9×9 nodal refinement is used at each crack tip. The mode I SIF obtained using the M-integral is compared with the results published in the literature. The auxiliary functions for the M-integral are derived from Sih et al. [63]. A comparison of the normalized SIF ($\tilde{K}_I = K_I / \sigma\sqrt{\pi a}$) is presented in Table 1.

Table 1 show that the results obtained using the proposed method reduces the need for higher nodal density if higher order Gauss integration is used. The result does not show much improvement beyond Gauss quadrature involving 16 Gauss points in the background triangular cells. As expected, the FEM requires more degrees of freedom (DOF) to obtain accurate SIF. The usage of enrichment functions decreases the DOF in the XFEM. When compared to XFEM, XEFG method requires relatively lesser DOF. However, by using a lower nodal refinement at the crack tip, an accurate SIF is obtained using the present method. This is mainly attributed to the ability of the EFG method's shape functions to reproduce higher order fields. The refinement process in the region around the crack tip is not computationally cumbersome as in the case of the FEM.

Fig. 9(b) shows an inclined crack in a rectangular plate of $L/w = 2$ and $a=\sqrt{2}$. Table 2 shows a good comparison between the mixed mode SIFs obtained by the present method and existing results in the literature.

Table 1. Normalized mode I SIF for a centre crack in a finite orthotropic plate.

Method	DOFs	Elements	Background cells	Gauss points in the triangular cells	$\tilde{K}_I$
FEM [64]	11702	2001	-	-	0.997
XFEM [65] -	4278	2025	-	-	1.018
XFEM [66] – Orthotropic enrichment	4278	2025	-	-	1.020
XEFG [67]	4035	-	1849	13	1.0045
Present Method – I	3644	-	1614	7	1.0416
Present Method - II	3644	-	1614	13	1.0161
Present Method - III	3644	-	1614	16	1.0072
Present Method - IV	3644	-	1614	37	1.0075
Present Method - V	3644	-	1614	48	1.0071

Table 2. Normalized mode I and II SIF for an inclined crack in a finite orthotropic plate.

Normalized SIF	Ref. [63]	Ref.[64] FEM	Ref.[66] XFEM	Ref. [67] XEFG	Ref. [68] FEM	Ref. [69] FEM	Present Method
$\tilde{K}_I$	0.5	0.506	0.514	0.512	0.484	0.485	0.509
$\tilde{K}_{II}$	0.5	0.495	0.519	0.530	0.512	0.498	0.510

6.2 Bi-material disk subjected to thermal loading

Fig. 10 shows a bi-material disk subjected to cooling i.e. ΔT =-5°C. The radius (r) of the disc is 20 mm and the crack length ($2a$) is $0.5r$. The upper material (1) is glass with $E_1 = 73\text{GPa}$, $\eta_1 = 8\text{e-}6/^{\circ}\text{C}$ and $v_1 = 0.22$; and the lower material (2) is epoxy with $E_2 = 2.9\text{GPa}$, $\eta_2 = 73\text{e-}6/^{\circ}\text{C}$ and $v_2 = 0.29$. A state of plane strain is assumed.

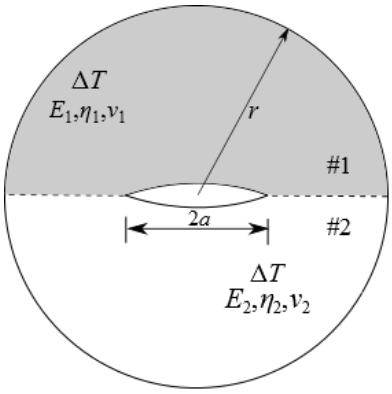

Fig. 10. Bi-material disc with central crack subjected to temperature change ΔT.

The complex SIF is calculated using the thermal interaction integral, Eq. (6). For the evaluation of the integral, a square domain with edge length of $0.25a$ is considered. The SIF obtained is

normalized as per $\tilde{\mathbf{K}} = \mathbf{K}L^{i\varepsilon}/\sigma\sqrt{\pi a}$; $\left(\mathbf{K} = K_1 + iK_2\right)$ where $\sigma = \dfrac{(1-\nu_1)\eta_1 - (1-\nu_2)\eta_2}{1/E_2^* - 1/E_1^*}\Delta T$ and $L = a.$

The reference results are: (1) $\tilde{K}_1$ =-0.3466 and $\tilde{K}_2$= 0.2389 by FEM [59]; (2) $\tilde{K}_1$ =-0.3523 and $\tilde{K}_2$= 0.2342 by the enriched EFG method [70]. The normalized SIFs obtained by the present method are $\tilde{K}_1$ = -0.3574 and $\tilde{K}_2$ = 0.2387. The results show that the present method, devoid of enrichment functions, is able to give the SIFs close to the results of [70] based on enrichment.

6.3 Bi-material interfacial edge crack in a finite plate

The dimensions of the plate studied (Fig. 11(a)) are: width $w = 1\,\text{m}$ and $L/w = 3$. The normal traction at the top and bottom edges is 1MPa. The plate is discretized with 21×61 nodes. The domain of influence is set at 1.75 times the nodal spacing. The material properties employed are as follows: $E_2 = 205.8\,\text{GPa}$; three ratios of $E_1/E_2 = 2$ and 100 are considered. The Poisson's ratio, $\nu = 0.3$, is set for both materials. A state of plane stress condition is assumed. The region around the crack tip is refined with 13×13 nodes (Fig. 11(b)).

Fig. 12 shows the convergence of K_1 and K_2 for an edge crack of length $a/\text{w} = 0.5$ for $E_1/E_2 = 2$. As the refinement increases around the crack tip, the solution converges indicating that the present EFG method is sufficient to analyze bi-material interface crack.

The normalized SIFs ($\mathbf{K}/\sigma\sqrt{\pi a}$) based on the proposed EFG method obtained for crack ratios (a/w) varying from 0.1 to 0.7 are compared (Fig. 13) with results available in the literature [62, 71-72]. These are also compared with those obtained by the XEFG method. Since the XEFG method incorporates special functions, the region around the crack tip was not refined with additional nodes.

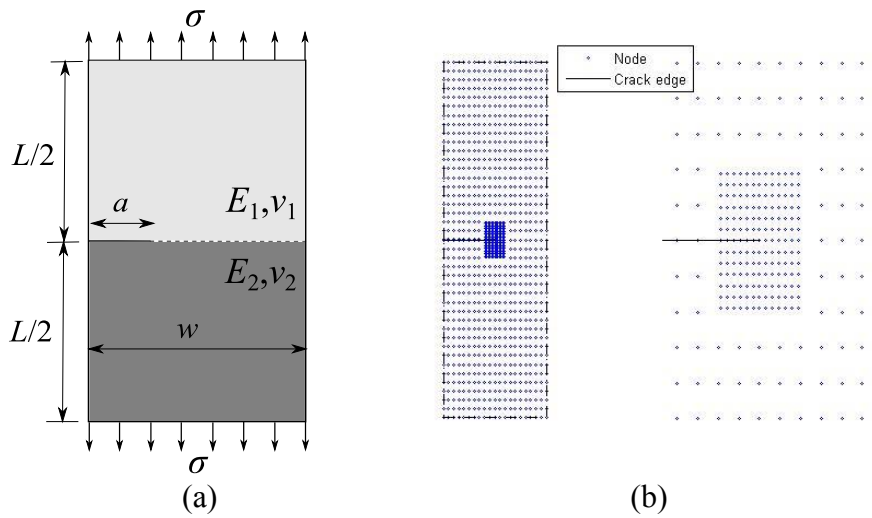

Fig. 11. (a) Interfacial edge crack in bi-material plate; **(b)** Nodal discretization.

The SIFs are obtained using the interaction integral involving crack tip auxiliary functions for the interface crack. A square domain of side length $0.125a$ centered on the crack tip is considered as the domain for the interaction integral. The results show that there is an excellent agreement with the published results and with those obtained by the XEFG method.

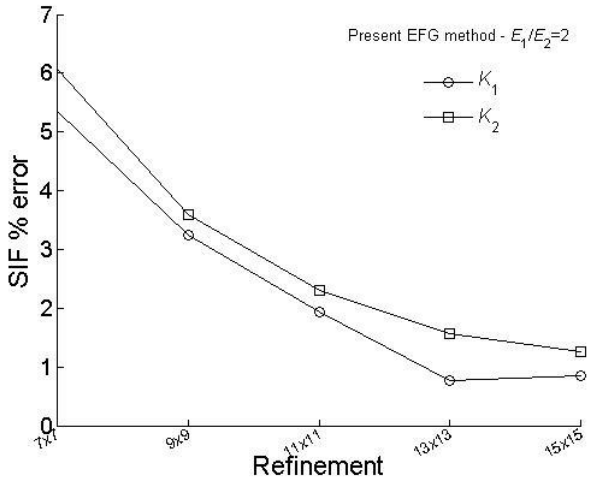

Fig. 12. % error in SIF with refinement in the region around the crack tip, using the present EFG method.

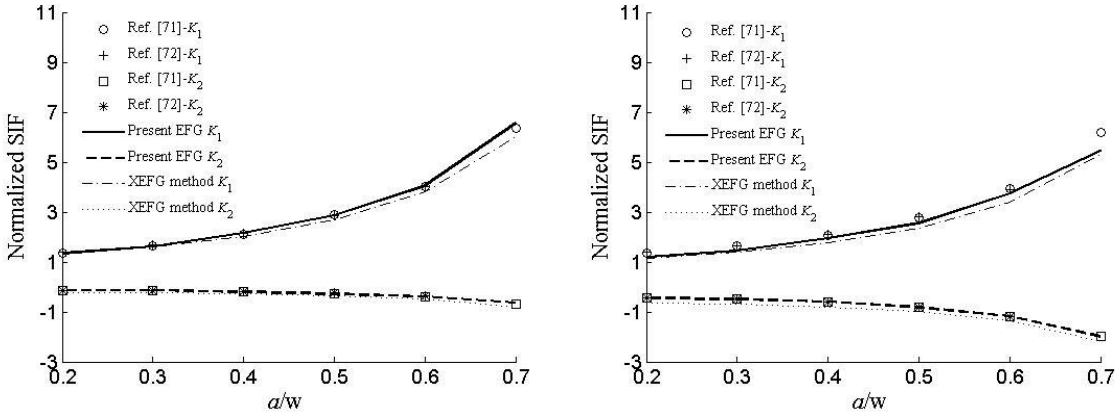

(a) (b)

Fig. 13. Comparison of normalized SIFs for **(a)** $E_1 / E_2 = 2$ and **(b)** $E_1 / E_2 = 100$.

Fig. 13 (a) and (b) show the similar comparisons of the normalized SIFs for $E_1 / E_2 = 2$ and $E_1 / E_2 = 100$ respectively. The results obtained by the proposed EFG method are in slightly in better agreement [71, 72] with those obtained through the XEFG method. This may be due to the refinement in the region around the crack tip. It is observed that the computed SIFs deviate slightly from the published results, as the ratio of E_1 / E_2 increases. The average error when compared with the published results [71] is less than 5%.

6.4 Orthogonal crack near material interface

Fig. 14 shows a bi-material panel with an internal crack where $a/w = 0.1$, $L/w = 3$, $w = 10\,\text{m}$, $\rho = \ln(10)/2w$ and $\sigma = 1\text{MPa}$. Material 1 is a functionally graded material and material 2 is an isotropic and homogenous material. A state of plane strain is assumed. Poisson's ratio $v = 0.3$ is set for both the materials. The value of E_0 is 1MPa. Two cases are considered: In case (1), a sharp material discontinuity (Young's modulus) exists at $x = 0$. While material 1 has modulus of E_0 very close to left side of the interface, material 2 has modulus of $2E_0$. In case (2) there is no material property discontinuity at $x = 0$, but their derivatives are discontinuous. The modulus of material 1 and 2 are E_0, just left and right to the

interface. The moduli of material 1 varies exponentially in both the cases

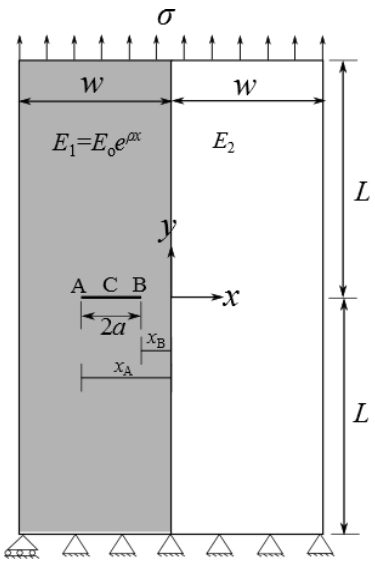

Case 1: $E_2=2E_o$ $(x \geq 0)$
Case 2: $E_2=E_o$ $(x \geq 0)$

Fig. 14. Crack terminating normally to material interface.

For a crack tip at the interface, $\sigma_{ij} \propto r^{\lambda-1}$ where λ is the order of the singularity; λ can have a single real value or two real or complex values depending on the material combination and angle of orientation of the crack with the interface. A method of calculating the SIF with good accuracy, using the proposed variant of the EFG method through the displacement method when the crack tip is at the interface, was presented in [73]. The usual interaction integral cannot be of any help in this case.

The normalized mode I SIFs ($K_{\mathrm{I}}/(\sigma\sqrt{\pi a})$) for crack tip at A and B are plotted in Fig. 15(a) and Fig. 15(b) respectively as the location of crack centre C is varied. Crack tip A and crack tip B meet the interface when $x_{\mathrm{A}}/w=0$ and $x_{\mathrm{B}}/w=0$ respectively. The interface is indicated by the dotted line.

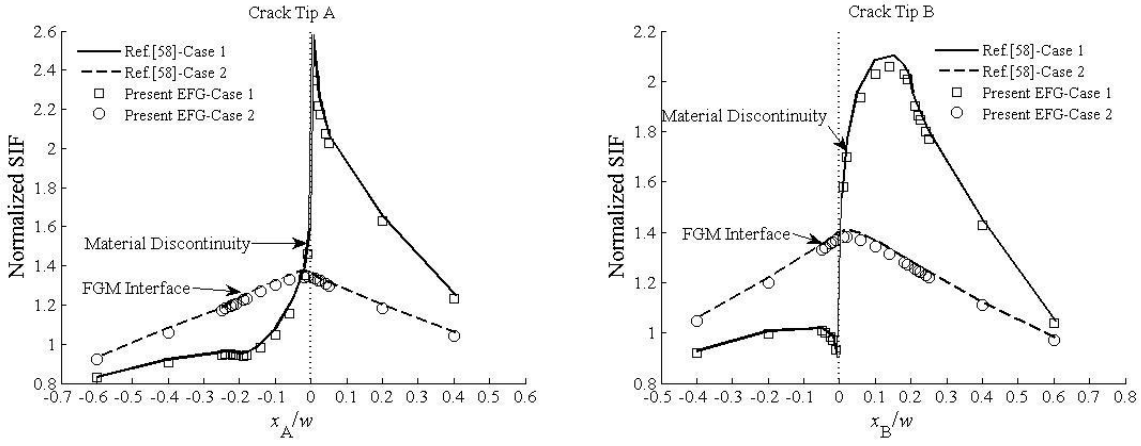

(a) (b)

Fig. 15. Variation of normalized mode I SIFs **(a)** crack tip A; **(b)** crack tip B.

Case (1) – Interface with sharp material discontinuity: The mode I SIF for crack tip A increases gradually as the tip approaches the interface from the left. When the tip is at a distance of about $x_{\mathrm{A}}/w=0.2$, i.e., tip is away from the interface by the crack size, the SIF starts dropping slowly, then rises rapidly because of the influence of the stiffer material 2. It picks up the maximum

value when $x_A / w \approx 0$. As soon as it moves into the material 2, its SIF has a sharp jump because of the material influence. Subsequently it drops. For the tip B, the SIF reaches maximum when it is almost away from the interface by $x_A / w = 0.1$. On further movement towards the interface, it drops to a lower level. As it crosses the interface, the SIFs jump to higher level and it continues until it is away from the interface by a distance equal to the crack size. Then it drops.

Case (2) – FGM Interface: In the case of an interface characterized by FGM behaviour, the SIFs for both the crack tip A and B increase until they meet the interface. As the crack cross the interface, the SIFs at both the tips starts dropping. Such a case study was reported earlier in [74]. The observations in the SIF variation, for both the cases, are consistent with the results of reference [58].

6.5 Crack meeting at an oblique angle to the material interface

Fig. 16 shows an edge crack inclined at an angle 20° to the *x*-axis with $L/w = 3, w = 0.5\text{m}$ and $\sigma = 1\text{MPa}$. A state of plane strain is assumed. Poisson's ratio, $v = 0.3$, is set for both the materials. The ratio of Young's moduli (E_1 / E_2) is set to 100. In this case, there are two orders of singularity: $\lambda_1 = 0.114$ and $\lambda_2 = 0.071$. A set of eight enrichment functions are needed for accurate modelling using XFEM or XEFG method.

The crack opening displacement (v_{COD}) profiles, obtained using the proposed EFG method and FEM are compared in Fig. 17(a). There is a good agreement between the two for $r > 0.01$. The results are obtained using 2860 DOF in the present method. In the case of FEM, 995596 DOF with 165794 eight-node quadrilateral elements are employed in ANSYS to obtain a converged solution. In the case of the FEM, a very fine mesh near the crack tip (crack tip element size – $0.005a$) and a coarse mesh away from it is employed. The improvement in performance in the case of the proposed EFG method is attributed to its higher order continuous shape functions.

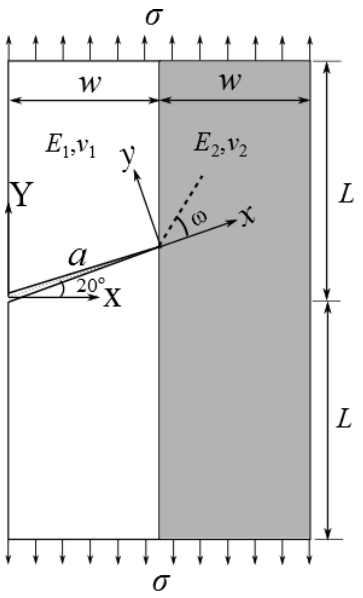

Fig. 16. Crack meeting at an angle to the bi-material interface.

In order to find the instantaneous angle of crack propagation, the ratio of the ERR ($G_{m\omega}$) along the kinking angle ω and the ERR (G_I) along the interface is plotted for various direction θ in Fig. 17 (b). As θ increases, $G_{m\omega} / G_I$ increases until θ=-20°. Afterwards, it decreases

steadily until at θ=70° when the crack is an interface crack . This plot shows that the crack will propagate at ω=θ=-20°, as the $G_{m\omega}/G_I$ ratio is maximum for this direction, if the interface is tough. This is in agreement with the results published in the case of a tough interface [75]. That means it will extend perpendicular to the applied load provided the interfacial fracture toughness is more than 0.36 times the material #2 fracture toughness ($\frac{\Gamma_f^I}{\Gamma_f^2} > \frac{1}{2.814}$).

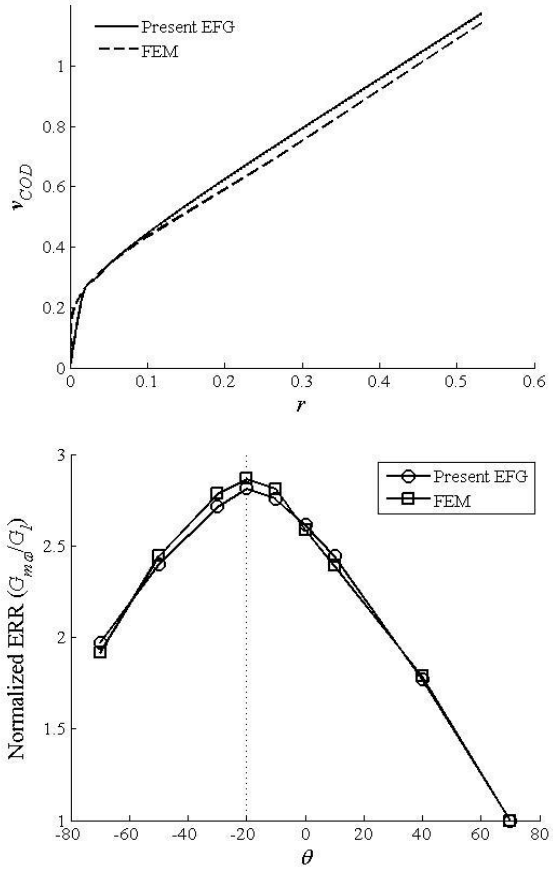

(a) (b)

Fig. 17. (a) Crack opening displacement for crack meeting the interface. **(b)** Variation of the ERR ($G_{m\omega}$)/ERR (G_I) with kink angle ω.

6.6 T-stress for crack in bi-materials

Two cases have been considered to illustrate the effectiveness of the proposed approach in evaluating T-stress. A state of plane strain condition is assumed in both the cases.

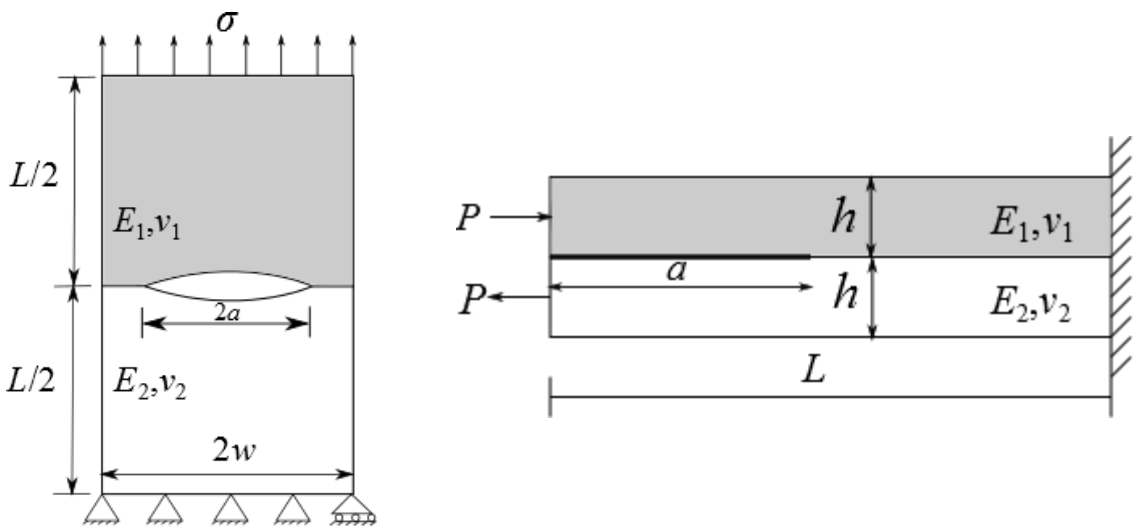

(a) (b)

Fig. 18. (a) Centre crack in bi-material plate; **(b)** Edge crack in a bi-material strip.

Case (a): A bi-material plate with a centre crack (Fig. 18(a)) is considered. The dimensions are: $L/w = 2$, $w = 1\text{m}$ and $\nu_1 = \nu_2 = 0.3$. The ratio of Young's moduli (E_1/E_2) is varied from 1 to 10. The T-stress is computed for three different crack length ratios (a/w): 0.15, 0.25 and 0.35. The plate is subjected to a uniform tensile load σ. The results obtained are compared with the results obtained by Sladek and Sladek [60]. The computed T-stress is normalized ($B = \text{T}/\sigma_o$) by σ_o, where

$$\sigma_o = [(K_1^2 + K_2^2)/\pi a]^{1/2} \tag{15}$$

The T-stress is obtained using the interaction integral using the appropriate auxiliary solutions. Taking note of the suggestion of a bigger integral domain [57] for T-stress calculation, a square domain with edge length of crack length a, is used. Fig. 19 shows that the normalized T-stress obtained by the proposed approach is in good agreement with the published results for various E_1/E_2 ratios.

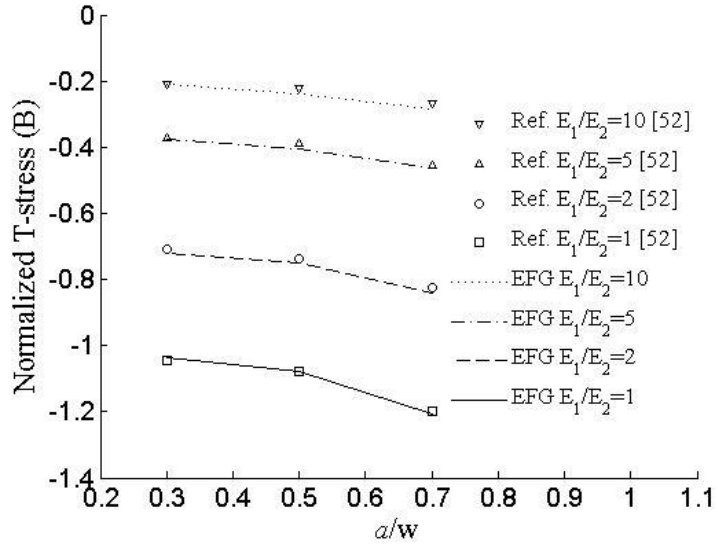

Fig. 19. Comparison of normalized T-stress for centre crack in bi-material plate subjected to uniaxial tension.

Case (b): A bi-material strip with an edge crack (Fig. 18(b)) is examined. The dimensions are: $a/L = 0.5$, $h/L = 0.1$ and $L = 10\text{m}$. The strip is subjected to point loads, $P = 1\text{MN}$, as shown in the figure. The right end of the strip is fixed. Table 3 presents comparisons of normalized T-stress, $\text{T}/(P/h)$, for different material combinations with the published results [57,76]. The comparison shows a good agreement with the reference results.

Table 3. Comparison of normalized T-stress for different material combinations for crack in bi-material strip.

E_1/E_2	ν_1	ν_2	α	β	$\text{T}/(P/h)$		
					Present EFG method	Ref [57]	Ref [76]
7/3	1/3	1/3	0.4	0.1	0.0709	0.0702	0.0709
20/9	1/4	1/8	0.4	0.2	0.0778	0.0773	0.0784
4	2/5	2/5	0.6	0.1	0.1301	0.1317	0.1310
4	1/4	1/4	0.6	0.2	0.1419	0.1410	0.1424

6.7 Interface crack kinking angle

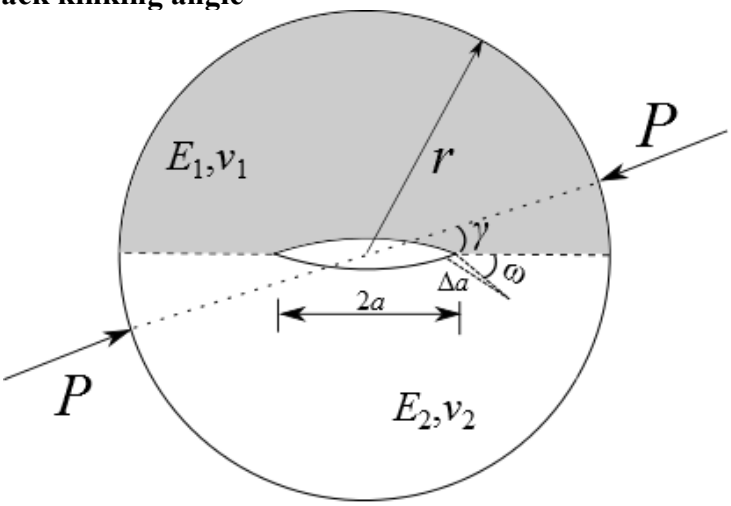

Fig. 20. Bi-material disc subjected to diametrical compression by point loads.

To predict the kink angle ω for an interface crack, a bi-material disc subjected to point loads, P, oriented at angle γ to the crack plane, is considered (Fig. 20). The dimensions are: $r =$ 40mm and $a/r = 0.25$. The material properties are appropriately chosen to vary α and β. The mode-ratio (ψ) is defined as

$$\psi = \tan^{-1}(K_2/K_1) \tag{16}$$

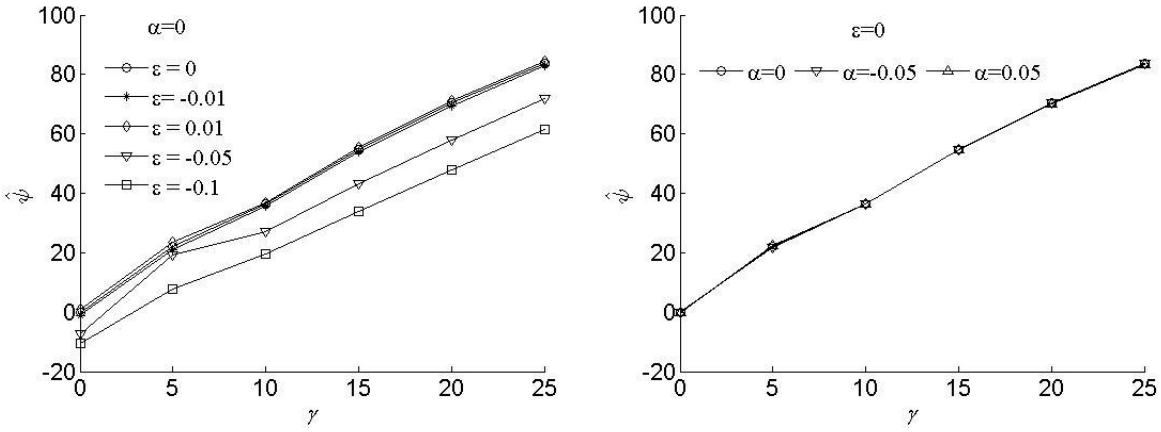

(a) (b)

Fig. 21. Variation of mode-ratio $\hat{\psi}$ with compression angle γ for **(a)** $\alpha = 0$ and various ε **(b)** $\varepsilon = 0$ and various α.

Fig. 21 shows the variation of mode-ratio ($\hat{\psi}$), where $\hat{\psi} = -\psi$, with the compression angle (γ) for different material combinations. The variation pattern of $\hat{\psi}$ with oscillation index ε, for $\alpha = 0$, as shown in Fig. 21(a), is similar to that of the results based on FEM reported in [77]. This shows that, as γ increases, the crack experiences higher mode-ratio $\hat{\psi}$. $\hat{\psi}$ for a particular γ is found to depend on ε and it decreases as ε decreases. When $\varepsilon = 0$, $\hat{\psi}$ does not depend on Dundurs' parameter, α, (Fig. 21(b)). This suggests that the kink angle ω is primarily dependent on ε. By means of extrapolation it is found that $\hat{\psi}$=90° at around $\gamma = 28°$, for small ε ($|\varepsilon| \le 0.01$). This is in close agreement with fracture test results of Atkinson et al. [78].

The variation of interface crack kink angle, ω, with ψ for various α when $\beta = 0$ is shown in Fig. 22 (a). This is plotted without consideration of the T-stress. The present results are in good agreement with the results obtained using the stress criterion by Yuuki and Xu [44]. They too showed that ω depended on ψ alone when $\varepsilon = 0$. However, He and Hutchinson [34], using the energy-based approach, showed that ω was a function of ψ and α when $\varepsilon = 0$. It is to be emphasized that the stress field in the region close to the crack tip is determined using the computed SIFs and the T-stress. The shear stress is then plotted along a circle of finite radius r_c to determine the direction of kink angle ω.

As expected, when the T-stress is included to predict ω, for the material combination $\alpha = 0$ and $\beta = 0$, ω is found to change with r/a ratio (Fig. 22 (b)). There is a maximum difference of around 25° between the kinking angle at $r/a = 0.0001$ and $r/a = 0.05$. The T-stress is negative in this case and it decreases the magnitude of the kinking angle. Such a pattern was observed earlier for bi-materials [33] and functionally graded materials [79].

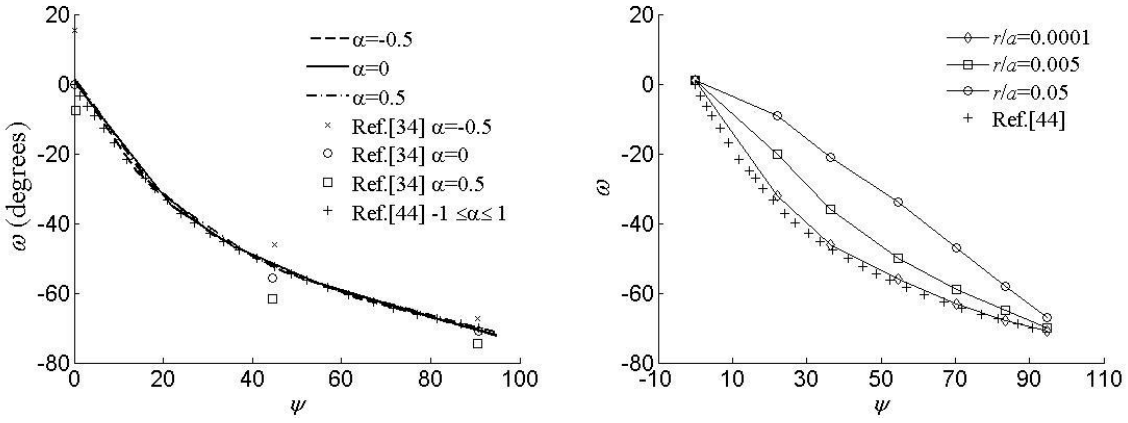

(a) (b)

Fig. 22. Predicted kinking angle for **(a)** various α without T-stress for $\beta = 0$ without T-stress and **(b)** various r/a ratios with T-stress for $\alpha = \beta = 0$.

Another factor that contributes to the varying kinking angle, ω, with r/a ratios is the oscillation index (ε). To illustrate the effect of ε, ω versus $\log_{10}(r/a)$ is plotted (Fig. 23 (a)) for different ε at $\gamma = 15^{o}$ without considering the effect of T-stress. It is observed that the slope of the plot is higher for a higher oscillation index indicating that ε plays an important role in determining the kinking angle.

The predicted kinking angle changes much more with the r/a ratio when the effect of T-stress is included, as shown in Fig. 23 (b). Both T-stress and ε affect the kink angle ω at a particular r/a ratio. It is observed that the crack does not kink for certain r/a ratios for $\varepsilon > 0.1$ ($\varepsilon = 0.125$ and $\log_{10}(r/a) < -3$, $\varepsilon = 0.175$ and $\log_{10}(r/a) < -2$). This is because on a circle of radius r around the crack tip, at which tangential and shear stresses are computed to determine ω, the maximum tangential stress is compressive. This is according to the corollary by Swedlow [80], who suggested that a crack propagates in the direction corresponding to the tensile stress. However, as r/a increases, the maximum tangential stress becomes tensile. The kink angles vary significantly with r/a when ε is large $(\varepsilon > 0.1)$, which was also showed in [44].

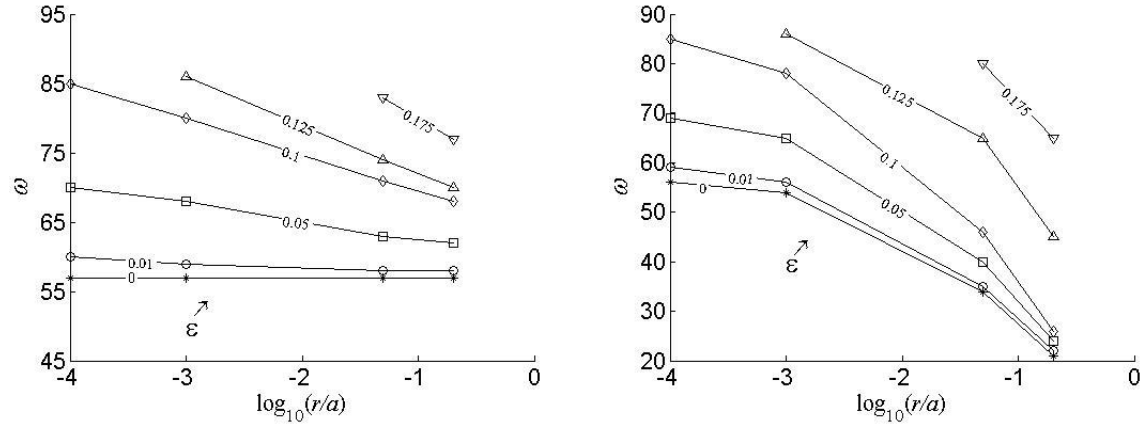

(a) (b)

Fig. 23. Variation of kinking angle with r/a ratios for different material combinations **(a)** without considering T-stress and **(b)** with considering T-stress.

6.8 Crack growth in the presence of particle reinforcement

A crack of length a is assumed to be present in a square plate of side L=2 m. The particle is of radius, $2r/L = 0.15$. The geometry is subjected to uniform tension of $\sigma = 1$MPa. Two arrangements of particles, Fig. 24(a) and Fig. 24(b), are studied. A state of plane strain is assumed. The particle material modulus is $E_p = 6.43E_m$. The particle and matrix Poisson's ratio are: $v_p = 0.17$ and $v_m = 0.33$ respectively. These values correspond to silicon carbide (SiC) particle reinforcement in aluminum (Al) matrix.

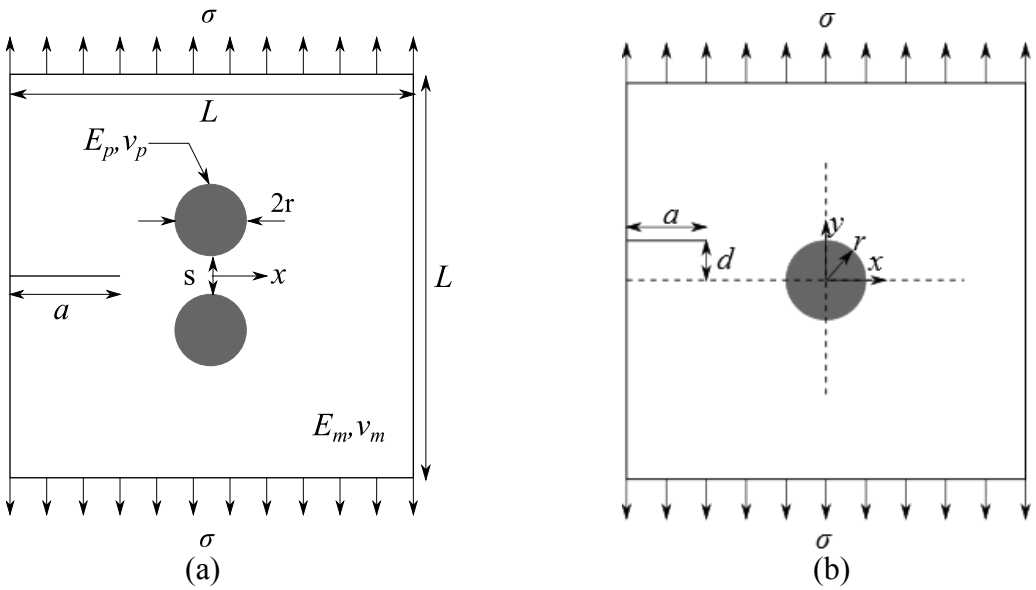

Fig. 24. (a) Cracked geometry with two particles. **(b)** Cracked geometry with single particle.

In the first case (Fig. 24(a)), the normalized energy release rate (G/G_o) is plotted as the crack propagates towards the particle starting from a crack size of $a = 0.4$. Such a crack size is chosen based upon previous work [81], which showed that the particle effect on the crack is insignificant when the distance of the crack tip from the particle centre is more than 4*r*. It is to be noted that the 'visibility method' is used to model the crack tip in the previous work. G is the energy release rate (ERR) for a propagating crack and G_o is the ERR for the same geometry in the homogenous matrix of aluminium.

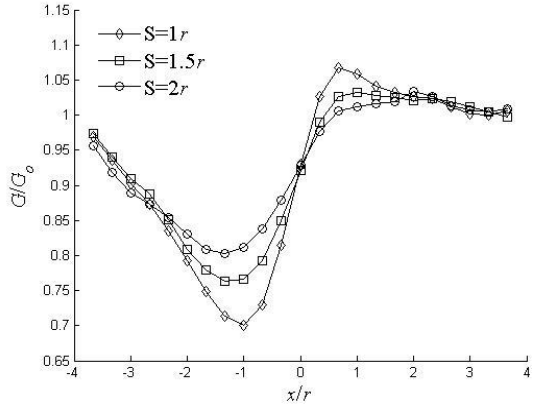

Fig. 25. Variation of normalized energy release rates with x/r for various S/r ratios for mode I crack in presence of two particles.

Inter-particle distance, S, is varied to show its effect on the propagation of a mode I crack. As

the crack approaches the particle, the effect of shielding and amplification is observed to vary with S. The shielding implies a decrease in G. Both the shielding and amplification effects are found to enhance with decreasing inter-particle distance (Fig. 25). The crack advancement length and the finite radius r_c at which the shear stress is plotted are the same ($r_c = 0.04$).

In the case of single particle reinforcement (Fig. 24(b)), the crack paths have also been determined. As the crack approaches the stiff particle, it gets repelled. The MTPS criterion, which includes the effect of the T-stress, has been employed to find the instantaneous angle of crack propagation and the crack path (Fig. 26(a)).

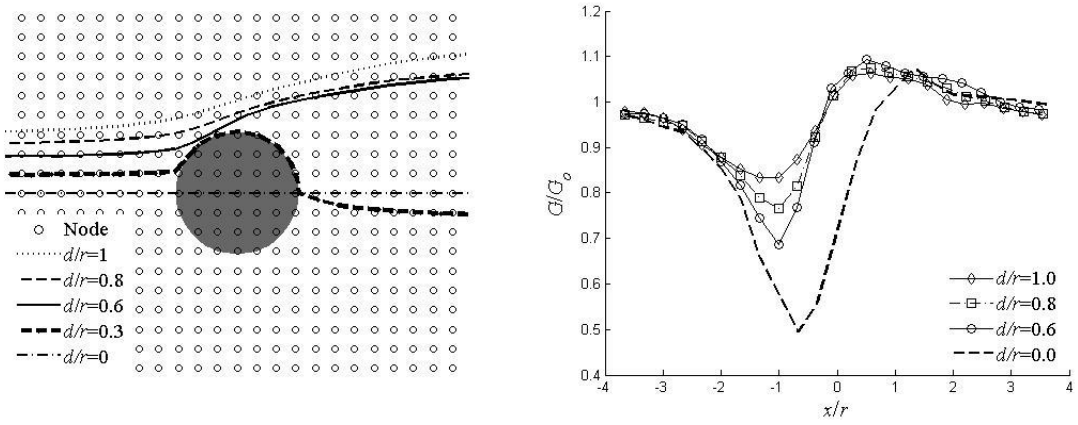

(a) (b)

Fig. 26. (a) Crack paths for various d/r ratios. **(b)** Variation of normalized energy release with x/r for various d/r ratio.

The variation of normalized ERR ratio (G/G_o) is plotted with normalized crack tip position (x/r) with respect to the particle centre in Fig. 26 (b). The normalized ERR variation as the crack propagated shows the shielding and the amplification effect. It was observed that the shielding effect was more pronounced than the amplification effect in the material combination and the properties considered.

This plot, for $d/r \geq 0.6$, matches closely with results presented in [82,83]. The crack experiences a shielding effect, i.e. a decrease in G/G_o, as it approaches the particle and amplification effect, i.e. an increase in G/G_o, as it moves away from the particle. As d/r decreases, these effects increase. The shielding effect can lead to a toughening mechanism. The inter-particle distance and/or proximity of the crack to the particle can be adjusted to result in a toughening mechanism.

The shielding effect is highly enhanced, for $d/r=0$, when a mode I crack approaches the particle. When this crack reaches the interface, it is likely to penetrate the particle if the interface fracture toughness is greater than 0.63 times the particle fracture toughness $\left(\Gamma_f^I > 0.63\Gamma_f^{SiC}\right)$ along $\omega=0^o$. Otherwise, it would propagate along the interface. It may or may not kink into the aluminium matrix depending on the $\Gamma_f^I / \Gamma_f^{Al}$ ratio. The effect of the particle on the crack is reduced as it moves away from the particle.

For $d/r=0.3$ (Fig. 26(a)), the crack propagates in the aluminium matrix up to the interface and then along the interface. It is observed that the crack approaches the particle at an angle close to 0^0 with respect to the interface. The crack then propagates along the interface and kinks out

of the particle-matrix interface. This kinking out is governed by the MTPS criteria in conjunction with the maximum energy release rate. If $\Gamma_f^I > 0.37\Gamma_f^{Al}$, the crack kinks into the relatively compliant ($\alpha = 0.71$) aluminium and extend as a normal crack in an isotropic and homogenous medium. The composite is assumed to contain no flaws. In reality, there may be flaws near the particle-matrix interface which will influence the evolution of the crack. Crack growth in a bi-material medium is complex and governed by many factors.

The crack propagation in this particle-reinforced composite involves a wide spectrum of possibilities. Depending on the relative interface fracture toughness (Γ_f^I) with respect to the toughness of the two materials and relative position of the crack with respect to the particle, fracture patterns may vary from interface cleavage/particle-matrix decohesion to particle breakage. The fracture toughness of the interface Γ_f^I varies with the contact time between the SiC particle and the molten Al matrix during the manufacturing stage [84]. The possibility of occurrence of various patterns of crack propagation studied here may have some correspondence to the practical situations.

CONCLUSION

The proposed variant of the Element-Free Galerkin (EFG) method guarantees results of satisfactory accuracy with a reduced number of degrees of freedom. It is a feasible method to model crack propagation in any material, as it does not require enrichment functions to model the crack tip. It can be employed for evaluation of LEFM parameters accurately. The SIFs obtained for a crack in the orthotropic material and bi-material interface crack under mechanical or thermal loading are in good agreement with the published results. The stress based MTPS criterion, that included T-stress, together with the energy-based approach reduces computational effort to determine the direction of kinking of an interface crack. The compressive T-stress is found to decrease the magnitude of the kinking angle. Both the T-stress and radial distance r_c, from the crack tip, affect the determination of the kinking angle. In the case of particle-reinforced composites, a wide spectrum of crack propagation possibilities exists. The important factors are relative positions of initial crack with respect to the particle centre, inter particle distance and fracture toughness of the interface and the toughness of the leading material. The tendency for a crack to grow along the interface or kink out of it depended on the relative standing of fracture toughness of the interface and the constituent materials.

Appendix A

The auxiliary displacement (u_i^{aux}), stresses (σ_{ij}^{aux}) and strains (ε_{ij}^{aux}) to determine T-stress are defined [60,58] by

$$
\begin{aligned}
u_1^{aux} &= -\frac{E^{\#} f}{E_o \pi}\left(2\ln\frac{r}{d} + (1+v_o)\sin^2\theta\right) \\
u_2^{aux} &= -\frac{E^{\#} f}{E_o \pi}\left((1-v_o)\theta - (1+v_o)\sin\theta\cos\theta\right) \\
\sigma_{11}^{aux} &= -E^{\#}\frac{2f}{r\pi}\cos^3\theta \\
\sigma_{22}^{aux} &= -E^{\#}\frac{2f}{r\pi}\cos\theta\sin^2\theta \\
\sigma_{22}^{aux} &= -E^{\#}\frac{2f}{r\pi}\cos^2\theta\sin\theta
\end{aligned}
\qquad \text{(A.1)}
$$

where f is a point force applied for auxiliary fields, d is a reference length and

$$
\begin{aligned}
&E^{\#} = \frac{E_o}{E_1^* + E_2^*}, E_o = E_m^* \forall \mathbf{x} \in \text{material } m \\
&v_o = v_m^* \forall \mathbf{x} \in \text{material } m \\
&v_m^* = \begin{cases} v_m \ \text{plane stress} \\ \dfrac{v_m}{1 - v_m} \ \text{plane strain} \end{cases}
\end{aligned}
\tag{A.2}
$$

The auxiliary strains are obtained using

$$
\varepsilon_{ij}^{aux} = S_{ijkl}(\mathbf{x}) \sigma_{kl}^{aux} \tag{A.3}
$$

where $S_{ijkl}(\mathbf{x})$ is the compliance matrix at the point $\mathbf{x}$.

REFERENCES

[1] M. Patrício, R.M.M. Mattheij "Crack paths in composite materials" *Engineering Fracture Mechanics*, 2010; **77**:2251-2262.

[2] D.B. Bogy, "On the plane elastostatic problem of a loaded crack terminating at a material interface" *Journal of Applied Mechanics,* 1971; **38**:911-918.

[3] Zhen Zhang, Zhigang Suo, "Split singularities and the competition between crack penetration and debond at a material interface" *International Journal of Solids and Structures*, 2007; **44**:4559-4573.

[4] T. Belytschko, T. Black, "Elastic crack growth in finite elements with minimal remeshing" *International Journal for Numerical Methods in Engineering,* 1999; **45**:601-620.

[5] Nicolas Moës, John Dolbow, Ted Belytschko, "A finite element for crack growth without remeshing" *International Journal for Numerical Methods in Engineering,* 1999; **46**:131-150.

[6] N. Sukumar, Z.Y. Huang, J.H. Prévost, Z. Suo, "Partition of unity enrichment for bimaterial interface cracks" *International Journal for Numerical Methods in Engineering*, 2004; **59**:1075-1102.

[7] S. Mohammadi, (2012) “XFEM fracture analysis of composites” (1st ed.), John Wiley and Sons, Ltd, p. 371.
[8] L. Bouhala, Q. Shao, Y. Koutsawa, A. Younes, P. Núñez, A. Makradi, S. Belouettar, “An XFEM crack-tip enrichment for a crack terminating at a bi-material interface” *Engineering Fracture Mechanics*, 2013; **102**:51-64.
[9] G.R. Liu, (2010) “Meshfree Methods: Moving Beyond the Finite Element Method”, (2nd ed.), CRC Press, p. 792.
[10] T. Belytschko, Y. Krongauz, D. Organ, M. Fleming, P. Krysl, “Meshless methods: An overview and recent developments” *Computer Methods in Applied Mechanics and Engineering*, 1996; **139**:3-48.
[11] T. Belytschko, Y.Y. Lu, L. Gu, "Element-Free Galerkin Methods" *International Journal for Numerical Methods in Engineering*, 1994; **37**:229-256.
[12] T. Belytschko, L. Gu, Y.Y. Lu, "Fracture and crack growth by element-free Galerkin methods" *Modelling and Simulation Material Science Engineering,* 1994; **2**:519-534.
[13] D. Organ, M. Fleming, T. Terry, T. Belytschko, "Continuous meshless approximations for non-convex bodies by diffraction and transparency", *Computational Mechanics,* 1996; **18**:225-235.
[14] Y. Krongauz, T. Belytschko, "EFG approximation with discontinous derivatives" *International Journal for Numerical Methods in Engineering,* 1998; **41**:1215-1233.
[15] T. Rabczuk, T. Belytschko, "Cracking particles: a simplified meshfree method for arbitrary evolving cracks" *International Journal for Numerical Methods in Engineering,* 2004; **61**: 2316-2343.
[16] G. Ventura, J.X. Xu, T. Belytschko, "A vector level set method and new discontinuity approximations for crack growth by EFG" *International Journal for Numerical Methods in Engineering,* 2002; **54**:923-944.
[17] Vinh Phu Nguyen, Timon Rabczuk, Stéphane Bordas, Marc Duflot, "Meshless methods: A review and computer implementation aspects" *Mathematica and computers in simulation,* 2008; **79**:763-813.
[18] M. Fleming, Y.A. Chu, B. Moran, T. Belytschko “Enriched element-free Galerkin methods for crack tip fields**”** in *International Journal for Numerical Methods in Engineering,* 1997; **40**:1483-1504.
[19] B.N. Rao, S. Rahman “An efficient meshless method for fracture analysis of cracks” *Computational Mechanics,* 2000; **26**:398-408.
[20] M. Duflot, H. Nguyen-Dang “A meshless method with enriched weight functions for fatigue crack growth” *International Journal for Numerical Methods in Engineering,* 2004; **59**:1945-1961.
[21] R. Namakian, H.M. Shodja, M. Mashayekhi “Fully enriched weight functions in mesh-free methods for the analysis of linear elastic fracture mechanics problems” *Engineering Analysis with Boundary Elements,* 2014; 43:1-18.
[22] N.T. Nguyen, T.Q. Bui , C. Zhang, T.T. Truong “Crack growth modeling in elastic solids by the extended meshfree Galerkin radial point interpolation method” *Engineering Analysis with Boundary Elements,* 2014; 44:87-97.
[23] J.G. Williams, P.D. Ewing, “Fracture under complex stress-the angled crack problem” *International Journal of Fracture,* 1972; **8**:441-446.
[24] I. Finnie, A. Saith, “A note on the angled crack problem and the directional stability of cracks” *International Journal of Fracture,* 1973; **9**:484-486.
[25] P.D. Ewing, J.G. Williams, “Further observations on the angled crack problem” *International Journal of Fracture,* 1974; **10**:135.
[26] Y. Ueda, K. Ikeda, T. Yao, M. Aoki, “Characteristics of brittle fracture under general combined modes including those under bi-axial tensile loads” *Engineering Fracture Mechanics* 1983; **18**:1131-1158.
[27] B. Cotterell “Notes on Paths and Stability of Cracks” *International Journal of Fracture*

Mechanics, 1966; **2**:526-533.
[28] D.J. Smith, M.R. Ayatollahi, M.J. Pavier "On the consequences of T-stress in elastic brittle fracture" *Proceedings of the Royal Society A: Mathematical, Physical and Engineering Science,* 2006; **462**:2415–2437.
[29] D.J. Smith, M.R. Ayatollahi, M.J. Pavier "The role of T-stress in brittle fracture for linear elastic materials under mixed-mode loading" *Fatigue and Fracture of Engineering Materials and Structures,* 2001; **24**:137-150.
[30] P.S. Leevers, J.C. Radon, L.E. Culver "Fracture trajectories in a biaxially stressed plate" *Journal of Mechanics and Physics of Solids,* 1976; **24**:381–395.
[31] N. Hallbäck, F. Nilsson "Mixed-mode I/II fracture behaviour of an aluminium alloy" *Journal of Mechanics of Physics and solids,* 1994; **42**:1345-1374.
[32] Y.G. Matvienko "Maximum Average Tangential Stress Criterion for Prediction of the Crack Path" *International Journal of Fracture,* 2012; **176**:113–118.
[33] Ki Ju Kang, "Criteria for kinking out of interface crack" *Engineering Fracture Mechanics,* 1994; **49**:587-598.
[34] M.Y. He and J.W. Hutchinson, "Kinking of a crack out of an interface" *Journal of Applied Mechanics,* 1989; **56**:270-278.
[35] B.K. Ahn, W.A. Curtin, T.A. Parthasarathy, R.E. Dutton "Criteria for crack deflection/penetration criteria for fiber-reinforced ceramic matrix composites" *Composites Science and Technology,* 1998; **58**:1775-1784.
[36] E. Martin, D. Leguillon, C. Lacroix, "A revisited criterion for crack deflection at an interface in a brittle bimaterial" *Composites Science and Technology,* 2001; **61**:1671-1679.
[37] E. Martin, D. Leguillon, C. Lacroix "An energy criterion for the initiation of interfacial failure ahead of a matrix crack in brittle matrix composites" *Composite Interfaces*, 2002; **9**:143-156.
[38] E. Martin, D. Leguillon, "Energetic conditions for interfacial failure in the vicinity of a matrix crack in brittle matrix composites" *International Journal of Solids and Structures,* 2004; **41**: 6937-6948.
[39] D. Leguillon, S. Tariolle, E. Martin, T. Chartier, J.L. Besson "Prediction of crack deflection in porous/dense ceramic laminates" *Journal of the European Ceramic Society*, 2006; **26**:343-349.
[40] E. Martin , B. Poitou, D. Leguillon, J. M. Gatt "Competition between deflection and penetration at an interface in the vicinity of a main crack" *International Journal of Fracture*, 2008; **151**:247-268.
[41] D. Leguillon , S. Murerb "A criterion for crack kinking out of an interface" *Key Engineering Materials*, 2008; **385-387**:9-12.
[42] A.R. Akisanya and N.A. Fleck, "Analysis of a wavy crack in sandwich specimens" *International Journal of Fracture,* 1992; **55:**29-45.
[43] M. Amestoy, J.B. Leblond "Crack paths in plane situations—II. Detailed form of the expansion of the stress intensity factors" *International Journal of Solids and Structures,* 1992; 29: 465-501.
[44] R. Yuuki and J.Q. Xu, "Stress based criterion for an interface crack kinking out of the interface in dissimilar materials" *Engineering Fracture Mechanics,* 1992; **41**:635-644.
[45] S.K. Maiti, R.A. Smith, "Comparison of the criteria for mixed mode brittle fracture based on the preinstability stress-strain field Part I: Slit and elliptical cracks under uniaxial tensile loading" *International Journal of Fracture,* 1983; **23**:281-295.
[46] P. Lancaster, K. Salkauskas, "Surfaces generated by moving least square methods" *Mathematics of Computation,* 1981; **37**:141-158.
[47] N. Moës, M. Cloirec, P. Cartraud, J.-F, Remacle, "A computational approach to handle complex microstructure geometries" *Computer Methods in Applied Mechanics and Engineering,* 2003; **192**:3163-3177.
[48] N. Muthu, S.K. Maiti, B.G. Falzon, I. Guiamatsia, "A comparison of stress intensity

factors through crack closure integral and other approaches using eXtended element-free Galerkin method" *Computational Mechanics,* 2013; **52**:587-605.
[49] N. Muthu, S.K .Maiti, B.G. Falzon, S. Khoddam, "Modified crack closure integral for extracion of SIFs in meshfree methods" *Finite Element in Analysis and Design,* 2014; 78:25-39.
[50] P.P.L. Matos, R.M. McMekking, P.G. Charalambides, M.D. Drory "A method for calculating stress intensities in bimaterial fracture" *International Journal of Fracture,* 1989; **40**:235-254.
[51] N. Miyazaki, T. Ikeda, T. Soda, T. Munakata "Stress intensity factor analysis of interface crack using boundary element method—Application of contour-integral method" *Engineering Fracture Mechanics,* 1993; **45**:599-610.
[52] T. Ikeda, C.T. Sun "Stress intensity factor analysis for an interface crack between dissimilar isotropic materials under thermal stress" *International Journal of Fracture,* 2001; **111**:229-249.
[53] J.F. Yau, S.S. Wang "An analysis of interface cracks between dissimilar isotropic materials using conservation integral in elasticity" *Engineering Fracture Mechanics,* 1984; **20**:423-432.
[54] T. Nagashima, Y. Omoto, S. Tani "Stress intensity factor analysis of interface cracks using X-FEM" *International Journal for Numerical Methods in Engineering,* 2003; **56**:1151-1173.
[55] H. Pathak, A.Singh, I.V. Singh "Numerical simulation of bi-material interfacial cracks using EFGM and XFEM" *International Journal of Mechanics and Materials in Design,* 2012; **8**:9-36.
[56] J.F. Yau, S.S. Wang, H.T. Corten, "A mixed-mode crack analysis of isotropic solids using conservation laws of elasticity" *Journal of Applied Mechanics,* 1980; **47**:335-341.
[57] Hongjun Yu, Linzhi Wu, Hui Li, "T-stress evaluations of an interface crack in the materials with complex interfaces" *International Journal of Fracture,* 2012; **177**:25-37.
[58] H.J. Yu, L.Z. Wu, L.C. Guo, S.Y. Du, Q.L. He, "Investigation of mixed-mode stress intensity factors for nonhomogeneous materials using an interaction integral method" *International Journal of Solids and Structures*, 2009; **46**: 3710-3724.
[59] Leslie Banks-Sills, Orly Dolev, "The conservative M-integral for thermal-elastic problems" *International Journal of Fracture,* 2004; **125**:1149-1170.
[60] J. Sladek, V. Sladek, "Evaluations of the *T*-stress for interface cracks by the boundary element method" *Engineering Fracture Mechanics,* 1997; **56**:813-825.
[61] S.K. Maiti, R.A. Smith, "Criteria for brittle fracture in biaxial tension" *Engineering Fracture mechanics,* 1984; **19**:793-804.
[62] Y. Murakami, "Stress Intensity Factors Handbook" *Oxford: Pergamon Press,* 1987.
[63] G.C. Sih, P.C. Paris, G.R. Irwin, "On cracks in rectilinearly anisotropic bodies" *International Journal of Fracture*, 1965; **1**:189-203.
[64] J.H. Kim, G.H. Paulino, "The interaction integral for fracture of orthotropic functionally graded materials: evaluation of stress intensity factors" *International Journal of Solids and Structures*, 2003; **40**:3967-4001.
[65] A. Asadpoure, S. Mohammadi, A. Vafai, "Modelling crack in orthotropic media using a coupled finite element and partition of unity methods" *Finite Element in Analysis and Design*, 2006; **42**:1165-1175.
[66] A. Asadpoure, S. Mohammadi, "Developing new enrichment functions for crack simulation in orthotropic media by the extended finite element method" *International Journal for Numerical Methods in Engineering,* 2007; **69**:2150-2172.
[67] S.S. Ghorashi, S. Mohammadi, S.-R. Sabbagh-Yazdi, "Orthotropic enriched element free Galerkin method for fracture analysis" *Engineering Fracture Mechanics,* 2011; **78**:1906-1927.
[68] S.N. Atluri, A.S. Kobayashi, M.A. Nagasaki, "Finite element program for fracture

mechanics analysis of composite material" *Fracture Mechanics of Composites ASTM STP,* 1975; **593**:86-98.
[69] S.S. Wang, J.F. Yau, H.T. Corten, "A mixed mode analysis of rectilinear anisotropic solids using conservation laws of elasticity" *International Journal of Fracture*, 1980; **16**:247-259.
[70] Mohit Pant, I.V. Singh, B.K. Mishra, "Numerical simulation of thermo-elastic fracture problems using element free Galerkin method" *International Journal of Mechanical Sciences*, 2010; **52**:1745-1755.
[71] T. Matsumto, M. Tanaka, R. Obara, "Computation of stress intensity factors of interface cracks based on interaction energy release rates and BEM sensitivity analysis" *Engineering Fracture Mechanics* 2000; **65**: 683–702.
[72] Mohit Pant, I.V. Singh, B.K. Mishra, "Evaluation of mixed mode stress intensity factors for interface cracks using EFGM" *Applied Mathematical Modelling* 2011; **35**:3443-3459.
[73] Nelson M. Muthu, Surjya K. Maiti and Wenyi Yan. "Analysis of Cracks in Bimaterials/Composites with Variable Order Singularity using Meshless Method" *World Congress on Computational Mechanics,* Barcelona, 2014.
[74] L.C. Guo, N. Noda, "Fracture mechanics analysis of functionally graded layered structures with a crack crossing the interface" *Mechanics of Materials,* 2008; **40**:81-99.
[75] Sundararajan Natarajan, Chongmin Song and Salim Belouettar, "Numerical evaluation of stress intensity factors and T-stress for interfacial cracks and cracks terminating at the interface without asymptotic enrichment" *Computer Methods in Applied Mechanics and Engineering,* 2014; **279**:86-112.
[76] J.H. Kim, J.J. Vlassak, "T-stress of a bi-material strip under generalized edge loads" in *International Journal of Fracture,* 2006; **142**:315-322.
[77] Zhijia Sun, Youtang Li, Hongyan Duan, "Consistent Mode Mixity for the Interface Crack of the Bimaterial Disc under Diametric Compression Loading" *Applied Mechanics and Materials,* 2013; **345**:268-271.
[78] C. Atkinson, R.E. Smelser, J. Sanchez, "Combined mode fracture via the cracked Brazilian disk test" *International Journal of Fracture,* 1982; **18**:279-291.
[79] Jeong-Ho Kim, Glaucio H. Paulino, "T-stress, mixed-mode stress intensity factors, and crack initiation angles in functionally graded materials: a unified approach using the interaction integral method" *Computer Methods in Applied Mechanics and Engineering,* 2003; **192**:1463-1494.
[80] J.L. Swedlow, "Criteria for growth of the angled crack" *Cracks and Fracture,* ASTM STP 601, American Society for Testing and Materials, 1976; 506-521.
[81] N. Muthu, B.G. Falzon, S.K. Maiti, S. Khoddam. "Modelling Crack Propagation in Particle-Reinforced Composites using the Element-Free Galerkin Method" *International Conference in Composite Materials*, Montreal, 2013.
[82] M.B. Bush, "The interaction between a crack and a particle cluster" *International Journal of Fracture,* 1997; **88**:215-232.
[83] Zhiyong Wang, Li Ma, Linzhi Wu and Hongjun Yu. "Numerical simulation of crack growth in brittle matrix of particle reinforced composites using the XFEM technique" *Acta Mech Solida Sinica,* 2012; **25**:9-21.
[84] L.M. Tham, M. Gupta, L. Cheng, "Effect of limited matrix-reinforcement interfacial reaction on enhancing the mechanical properties of aluminium-silicon carbide composites" *Acta Materialia*, 2001; **49**:3243-3253.